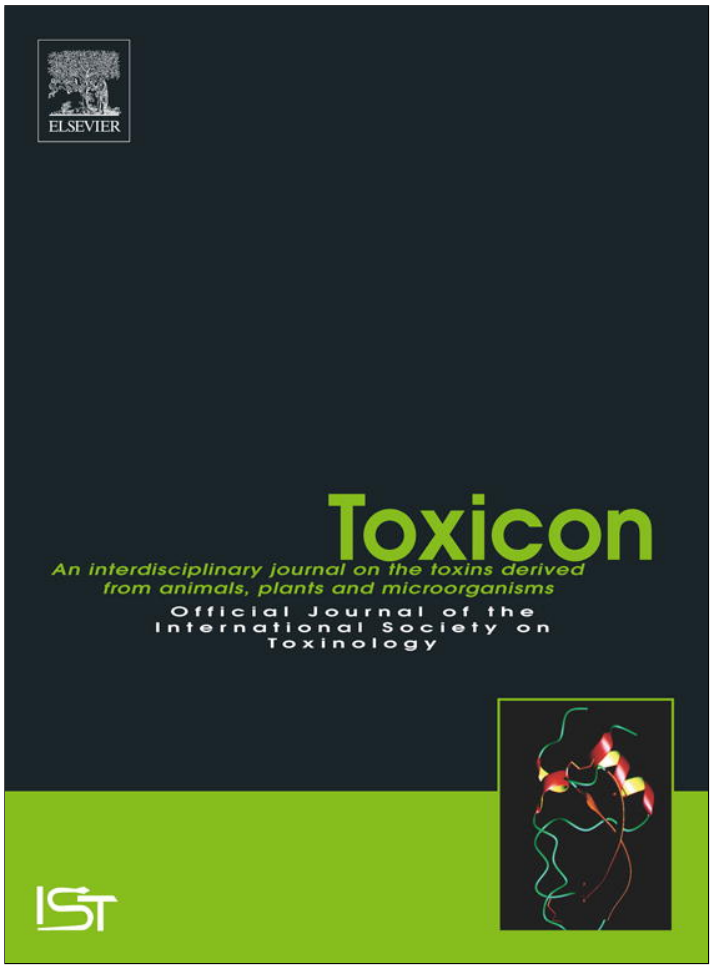

(This is a sample cover image for this issue. The actual cover is not yet available at this time.)

Toxicon 61 (2013) 83–93

Contents lists available at SciVerse ScienceDirect

Toxicon

journal homepage: www.elsevier.com/locate/toxicon

Effect of the disintegrin eristostatin on melanoma–natural killer cell interactions

Stefan Hailey [a], Elizabeth Adams [b], Ryan Penn [a], Alice Wong [c], Mary Ann McLane [a,*]

[a] Department of Medical Laboratory Sciences, University of Delaware, Newark, DE, USA
[b] Institute of Medical Sciences, University of Aberdeen, UK
[c] University of Maryland Hospital, Baltimore, MD, USA

ARTICLE INFO

Article history:
Received 28 February 2012
Received in revised form 17 October 2012
Accepted 23 October 2012
Available online 9 November 2012

Keywords:
Disintegrin
Melanoma
Natural killer cell
Atomic force microscopy

ABSTRACT

Malignant melanoma is difficult to treat due to its resistance to chemotherapeutic regimens. Discovery of new pharmaceuticals with inhibitory potential can be helpful in the development of novel treatments. The snake venom disintegrin eristostatin, from the viper *Eristicophis macmahoni*, caused immunodeficient mice to be significantly protected from development of lung colonization when melanoma cells and the disintegrin were co-injected *in vivo* into the lateral tail vein compared to vehicle controls. Cytotoxicity assays suggested that eristostatin makes the melanoma cells a better target for lysis by human natural killer cells. Direct binding assays using atomic force microscopy showed eristostatin does specifically bind the surface of the six melanoma cell lines tested. Eristostatin binding was partially inhibited by the addition of soluble RGDS peptide, suggesting an integrin as one likely, but not the sole, binding partner. Studies done with melanoma cells on a culture dish and natural killer cells attached to a cantilever tip in atomic force microscopy showed four major populations of interactions which exhibited altered frequency and unbinding strength in the presence of eristostatin.

1. Introduction

Malignant melanoma incidence rates have consistently increased over the past 35 years affecting men and women of all ages and ethnicities. It is estimated that in 2010 approximately 68,000 people were diagnosed with melanoma and almost 8700 cases were fatal (Howlader et al., 2011). Currently, the estimated lifetime risk of developing melanoma is 1 in 58 and this is expected to reach 1 in 50 by 2015 (Rigel et al., 2010). With growing occurrence it is of utmost importance to discover novel strategies for melanoma therapies.

Natural Killer (NK) cells are large granular lymphocytes which are principally responsible for the innate immune response in mammals (Zimmer, 2010). They have three major functional characteristics: cytotoxicity, cytokine and chemokine secretion, and contact-dependent cell costimulation. The cytotoxicity of NK cells is dependent on a balance between activation and inhibitory signals. A shift in this balance due to changes in activating receptors such as NKG2D, its ligand, MHC-class I chain-related protein A or B (MICA and MICB), or inhibitory receptors which recognize MHC-class I, can alter NK cytotoxicity (Zimmer, 2010).

Eristostatin (Er) is a short monomeric disintegrin isolated from the venom of *Eristicophis macmahoni*. It caused significant inhibition of lung and liver metastases due to B16F1 murine melanoma cells in an experimental metastasis model using C57BL/6 mice (Beviglia et al., 1995; Morris et al., 1995). Danen et al. (1998) observed that eristostatin inhibited lung colonization by human melanoma

* Corresponding author. Department of Medical Laboratory Sciences, University of Delaware, WHL305G, Newark, DE 19716, USA. Tel.: +1 302 831 8737; fax: +1 302 831 4180.
E-mail address: mclane@udel.edu (M.A. McLane).

0041-0101/$ – see front matter © 2012 Elsevier Ltd. All rights reserved.
http://dx.doi.org/10.1016/j.toxicon.2012.10.011

MV3, and we expanded these findings following an intravenous injection of eristostatin with MV3, M24met, or C8161 human melanoma cells into nude mice deficient in T and B cells but not deficient in natural killer cells (Danen et al., 1998; McLane et al., 2003). A set of function-blocking experiments, using antibodies for both α_v and β_1 showed substantial heterogeneity among five melanoma cell lines in their ability to adhere to eristostatin-coated plates. This evidence may indicate that eristostatin may act through a unique non-RGD dependent mechanism (Tian et al., 2007) or via integrins not tested. Exploring eristostatin's mode of action in the inhibition of metastases, McLane et al. showed that the cytotoxic effect of NK-like TALL-104 cells (O'Connor et al., 1991; Cesano and Santoli, 1992) increased when eristostatin was added to SBcl2 melanoma cells and/or the TALL-104 cells (McLane et al., 2001). However, the mechanism by which eristostatin acts on murine and human melanoma cells (or NK cells) is still unknown.

In the last decade major improvements have been made in techniques designed to measure cell–cell, cell–matrix, and receptor–ligand interactions. These interactions are dependent largely on adhesion molecules such as integrins and play a large role in many cell functions such as cell communication, migration and tumor metastasis (Desgrosellier and Cheresh, 2010). Atomic force microscopy (AFM) belongs to a broad group of instruments called scanning probe microscopes used to image and characterize the properties of material, chemical, and biological surfaces at the atomic scale and in three dimensions, *x*, *y*, and *z* (Blanchard, 1996). A common AFM technique used to measure the strength of interactions between a sample and the AFM tip is force spectroscopy. This requires the cantilever tip to approach and retract from the sample surface causing the cantilever to deflect. A laser is focused on the back of the cantilever, which follows this deflection and is used to quantify laser movement via a photodiode. This interaction is commonly expressed as unbinding force (nano Newtons, nN), the force released between two adhering molecules when those molecules are successfully moved apart. Through this relationship, AFM allows for the direct quantitative measurement of attractive and repulsive forces at the molecular level (Han and Serry, 2008; Benoit and Gaub, 2002).

The hypothesis for this project was that eristostatin would bind the surface of each melanoma cell, causing changes in the interactions between the melanoma cell and the natural killer cell. To test this hypothesis, force spectroscopy, using the atomic force microscope, confirmed that eristostatin bound each melanoma cell line's surface and characterized the unbinding interactions, specifically determining if those interactions were RGD-dependent. In addition, the effect of eristostatin on the unbinding characteristics of the melanoma cell–natural killer cell interactions were examined.

2. Materials and methods

2.1. Materials

Human melanoma cell lines 1205Lu (metastatic), WM164 (vertical growth phase), and SBcl2 (radial growth phase) were provided by Dr. Meenhard Herlyn (Wistar Institute, Philadelphia, PA). Metastatic cell lines C8161 and MV3 were acquired from Fred Meyskens (University of California, Irvine Cancer Center) and Goos N.P. van Muijen (University Medical Center, Nijmegen, Netherlands), respectively. The M24met (metastatic) cell line was provided by Ralph Reisfeld (The Scripps Institute, San Diego, CA). Dulbecco's Modified Eagle's medium/Ham's F12 50:50 mix (DMEM/F12), RPMI-1640 medium, and Dulbecco's phosphate buffered saline (DPBS) were purchased from Mediatech (Manassas, VA). Fetal bovine serum (FBS) was from GibcoBRL (Rockville, MD). Thrombin was obtained from Sigma (St. Louis, MO). RosetteSep Human NK cell enrichment cocktail and Ficoll–Paque PLUS were from Stemcell Tech (Tukwila, WA) and GE Healthcare (Piscataway, NJ), respectively. Anti-human CD-56 FITC conjugate was from Invitrogen (Carlsbad, CA), and mouse IgG2a FITC, clone CBL601F, was purchased from Cymbus Biotech (Hampshire, UK). Synthetic RGDS peptide was from ABBIOTECH (San Diego, CA). Atomic force microscopy tips were pyrex-nitride triangular cantilevers obtained from Nano World Innovative Technologies (Neuchâtel, Switzerland) and silicon nitride tips from Bruker (Camarillo, CA). Hydrogen peroxide (30% w/w) and sulfuric acid were purchased from Sigma (St. Louis, MO), glutaraldehyde (25%, Electron Microscopy grade) and ethanol were from Electron Miscroscopy Science (Hatfield, PA). Human interleukin-2 (IL-2) was purchased from Pepro Tech, Inc. (Rocky Hill, NJ). FITC-labeled concanavalin A was obtained from EY laboratories Inc. (San Mateo, CA). Eight chambered borosilicate coverslips (Lab-Tek II, #1.5) were obtained from Fisher Scientific (Bridgewater NJ). Highly specific and fluorescent-labeled monoclonal antibodies raised against integrin subunits α2, α5, α6, β1, β3 and the integrin αvβ3 were purchased from Chemicon (Temecula, CA). Fluorescein isothiocyanate (FITC) conjugated antibody to the α4 integrin subunit was purchased from Immunotech (Marsailles, France), while a FITC-stained antibody to αIIb was obtained from Cymbus Biotechnology (Chandlers Ford, United Kingdom).

2.2. Cell culture

All human melanoma cell lines were maintained in DMEM/F12 with 10% FBS at 37 °C and 5% CO_2. For atomic force microscopy, cells were grown to 80–100% confluence, detached using 2 mM EDTA, and transferred to a 60 mm cell culture plate and incubated overnight in DMEM/F12 containing 10% FBS at 37 °C and 5% CO_2.

2.3. Natural killer cell isolation

Natural killer cells were isolated using the RosetteSep method. Briefly, whole blood was collected in sodium heparin (143 U.S. Pharmacopeia units) to which RosetteSep Human NK enrichment cocktail was added. After mixing gently, the blood was incubated at room temperature (RT) for 20 min. The sample was diluted with an equal volume of PBS-2% FBS that was equilibrated to RT and mixed gently. In two new 50 mL conical tubes, 20 mL of blood/PBS were layered on top of 15 mL RT Ficoll–Paque and centrifuged at

1200 g for 20 min at RT. After centrifugation, the top plasma layer was aspirated and NK cells from each conical tube were removed from the plasma/Ficoll–Paque interface. The NK cells from both tubes were combined, washed with an equal volume of PBS-2% FBS and centrifuged at 300 g for 10 min. The NK cells were resuspended in five mL RPMI/10% FBS, stimulated with 750 IU/mL of IL2, and incubated at 37 °C and 5% CO_2 until use. If the NK cells were not used within 48 h of isolation they were restimulated with IL2 prior to use. For verification of the purity of the isolated cell population, the NK cells were analyzed using an Accuri C6 flow cytometer (Ann Arbor, MI) via an anti-human CD56 FITC conjugated antibody against an IgG2a isotype control.

2.4. Preparation of recombinant eristostatin

The expression of recombinant eristostatin in *Escherichia coli* was accomplished via a modification to a previously described method (Wierzbicka-Patynowski et al., 1999). This method was modified using the pET 39b (+) expression plasmid and the use of the His*Bind column (Novagen, Madison, WI) for the isolation and thrombin-cleavage of the 6-histidine fusion protein. Eristostatin was finally purified using high performance liquid chromatography (HPLC) on an Agilent 1100 series system (Santa Clara, CA) using a 5–60% gradient of acetonitrile in 0.02% trifluoroacetic acid (2 mL/min over 50 min).

2.5. Platelet aggregation

Eristostatin activity was confirmed by performing ADP-induced (20 μM) platelet aggregation in a whole blood aggregometer from Chrono-Log Corp. (Havertown, PA). Human subject protocol approval was obtained by the University of Delaware Human Subjects Review Board in January 1998 and renewed in 2012 (#154213-3). Aspirin-free blood was collected from healthy donors in 3.2% (w/v) sodium citrate (1:9 ratio). Percent aggregation inhibition was determined by subtracting the sample resistance value from the control resistance value, dividing by the control resistance value, and multiplying by 100. The percent inhibition and the concentration of the eristostatin were compared in Excel using a linear regression formula and the concentration of recombinant eristostatin that inhibited platelet aggregation by 50% (IC_{50}) was determined.

2.6. Atomic force microscopy

Silicon nitride probes with nominal spring constants of 0.01–0.5 N per meter (N m^{-1}) were cleaned with a piranha solution (30:70, H_20_2:H_2SO_4) prior to functionalization. Surfaces of the AFM probes were silanized using a 4% solution of 3-aminopropyltrimethylethoxysilane in 95% ethanol for 1 h at room temperature (RT). Probes were washed in ethanol (>99.9%), dried for 5 min at 100 °C, incubated for 10 min in 1.25% glutaraldehyde and washed in water. For blocking experiments, tips were incubated overnight at 4 °C in Er (0.1 mg/mL), and stored in PBS at 4 °C until used. For NK experiments, tips were incubated with either concanavalin A (0.1 mg/mL) or anti-human CD56 FITC conjugated antibody (0.2 mg/mL) and brought into contact for 5 min with a culture of NK cells stimulated with IL2. Tips were withdrawn from the surface and an inverted light microscope was used to confirm the presence of a single NK cell. The plate of NK cells was removed and replaced by a plate of test melanoma cells for measurement of force curves. In some experiments, the melanoma cells were pre-incubated with 500 nM Er or 200 μM of a synthetic RGDS peptide for 30 min at RT before force curves were measured. Literature for use of RGDS peptides for adhesion studies suggested using a concentration in the mM range (Dehio et al., 1998; McCarthy et al., 1986); however, it was observed that, with higher concentrations, the cells no longer remained attached to the surface of the culture plate. PicoForce contact mode was used for all measurements. Approximately 1000 forces curves were performed on 3 different cells. Of these, approximately 333 were performed at different areas on each cell, to make sure that the sampling was representative of the entire cell surface. To confirm repeatability, three separate AFM probes were used for each experimental condition. The distribution, average and standard error measurements were determined from these binding events and expressed in nanoNewtons (nN).

2.7. Confocal studies

Three hundred thousand melanoma cells, in DMEM with 10% fetal bovine serum (FBS), were incubated in an eight-chambered slide. Without washing, the cells were stained with FITC-labeled eristostatin ± varying concentrations of unlabeled eristostatin or with a FITC-labeled antibody to the specific integrin subunit being studied. All data were acquired on a Zeiss inverted 100M Axioskop equipped with a Zeiss 510 LSM confocal microscope and a krypton–argon laser. Acquisition of the fluorescein-conjugated probe used the 488 nm laser excitation line with a 500 nm long pass filter for fluorescence collection. Observations were taken at 400×. The images included are representative of a minimum of 2 identical experiments.

2.8. Labeling of eristostatin with FITC

FITC-Er was prepared as described (McLane et al., 1994). The FITC–peptide ratio was 1.2:1, and the final concentration of eristostatin was 0.5 μg/mL (93 nM). Platelet aggregation inhibitory activity (IC_{50}) of the FITC-Er was identical with that of unlabeled peptide.

2.9. Flow cytometry

To test the purity of NK cells isolated using the RosetteSep method, 300 μL of the NK-RPMI/10% FBS mixture was transferred into 3 wells of a v-bottomed 96-well plate. NK cells were spun for 30 s at 100 g and the supernatant decanted. Cells were washed (2×) in PBS-2% FBS with centrifugation for 30 s at 100 g. NK cells were resuspended in PBS-2% FBS and incubated for 10 min with PBS-2% FBS, IgG2a, or FITC-labeled anti-human CD56 antibodies for unstained, isotype control, and CD56-stained treatments, respectively. The samples were strained into tubes for cytometric analysis.

One million human melanoma cells, in DMEM, were washed three times with 1× binding buffer (10 mM N-(2-hydroxyethyl)piperazine-N′-2-ethanesulfonic acid (HEPES)/NaOH, pH 7.4, 140 mM NaCl, 2.5 mM $CaCl_2$). The cells were transferred to 12 × 75 mm tubes with a minimum of 0.5 mL 1× binding buffer and incubated with 3000 nM of unlabeled disintegrin. FITC-labeled antibody to the specific integrin subunit being studied was then added to each tube and incubated for at least 30 min in the dark. All data were acquired using a Becton Dickinson FACs Calibur or an Accuri C6 flow cytometer. For each cell line, treatments were done in triplicate.

2.10. Statistical analysis

A Student's *t*-test was applied to the data to determine the significant differences between the average unbinding forces detected. A *p*-value <0.05 was considered significant.

3. Results

3.1. Platelet aggregation

The IC_{50} values (mean ± SEM) for eristostatin ($n = 9$) was 48.2 ± 14.5 nM. These values were similar to those previously reported (McLane et al., 2004).

3.2. Direct unbinding of eristostatin and human melanoma cells

Atomic force microscopy was used to characterize the unbinding force interactions between eristostatin and the surface of the melanoma cell lines. Eristostatin bound all six melanoma cell lines tested with varying unbinding strengths (Fig. 1). This interaction was partially inhibited with the addition of 500 nM soluble eristostatin in the media causing a significant decrease in the unbinding force between eristostatin and C8161, MV3, M24met, and SBcl2 cell lines. 1205Lu and WM164, however, did not show any significant changes in unbinding force after the addition of the soluble eristostatin. These two cell lines also did not show a decrease in the percentage unbinding events compared to the total number of contacts after incubation with eristostatin, while the other four cell lines did (data not shown).

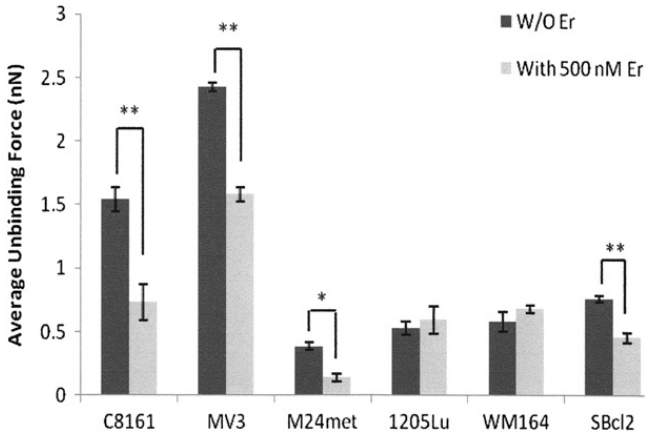

Fig. 1. Average unbinding force between melanoma cells and eristostatin on the AFM cantilever tip. Eristostatin functionalized tips were brought into contact with indicated melanoma cell lines incubated for 30 min in the presence or absence of 500 nM eristostatin. Data is mean unbinding force ± SEM from at least three experiments; $^{*}p = <0.05$; $^{**}p = <0.0001$; Er = eristostatin.

Histograms of these interactions (Fig. 2A–F) in the presence and absence of soluble eristostatin showed trends which are not obvious in Fig. 1. While changes in unbinding force were seen in the presence of eristostatin with every cell line, two things to note are (1) the variability and (2) the lack of one pattern of the unbinding forces observed when eristostatin was added.

3.3. Inhibition of the eristostatin–melanoma cell interaction by RGDS peptide

To determine the possibility of an integrin binding partner, cells were incubated in the presence or absence of a synthetic RGDS peptide. Of the six cell lines, five showed inhibition which was significant (Fig. 3).

This data was also visualized using histograms (Fig. 4A–F). An obvious decrease in unbinding force in the presence of RGDS appears with C8161 at 3 nN (Fig. 4A), with MV3 and WM164 at 1 nN (Fig. 4B, E) while there are smaller decreases (SBCl2, Fig. 4F) and even increases of unbinding force (MV3, M24met, 1205Lu, Fig. 4B–D) with the other cell lines.

3.4. Purity of freshly isolated natural killer cells

Natural killer cell populations isolated from freshly collected heparinized whole blood exhibited ≥90% purity when analyzed by flow cytometry using anti-CD56 (data not shown).

3.5. Direct unbinding of natural killer cell–melanoma cells

To determine any changes in the interactions between the melanoma cells and natural killer cells due to eristostatin, direct force measurement assays using AFM were done in the presence and absence of 500 nM eristostatin. In the case of all six human melanoma cell lines, the natural killer cells attached to the AFM cantilever tip (Fig. 5), and interacted with the surface of the melanoma cells (Fig. 6). After the addition of eristostatin, MV3 and WM164 showed a significant increase in the unbinding force between their surface and the natural killer cells, whereas M24met and SBcl2 displayed a significant decrease. C8161 and 1205Lu did not show any significant difference in the mean unbinding forces after the addition of eristostatin compared to the control.

Similar to the histograms in Figs. 2 and 4, the histograms of the unbinding forces which occurred between the natural killer cells and melanoma cells showed varying patterns in treatments with and without eristostatin. In general, decreases in unbinding forces were seen (C8161, M24met, SBCl2, Fig. 7A, C, F) while in three instances, increases in unbinding force were observed (MV3, 1205Lu, WM164, Fig. 7B, D, E).

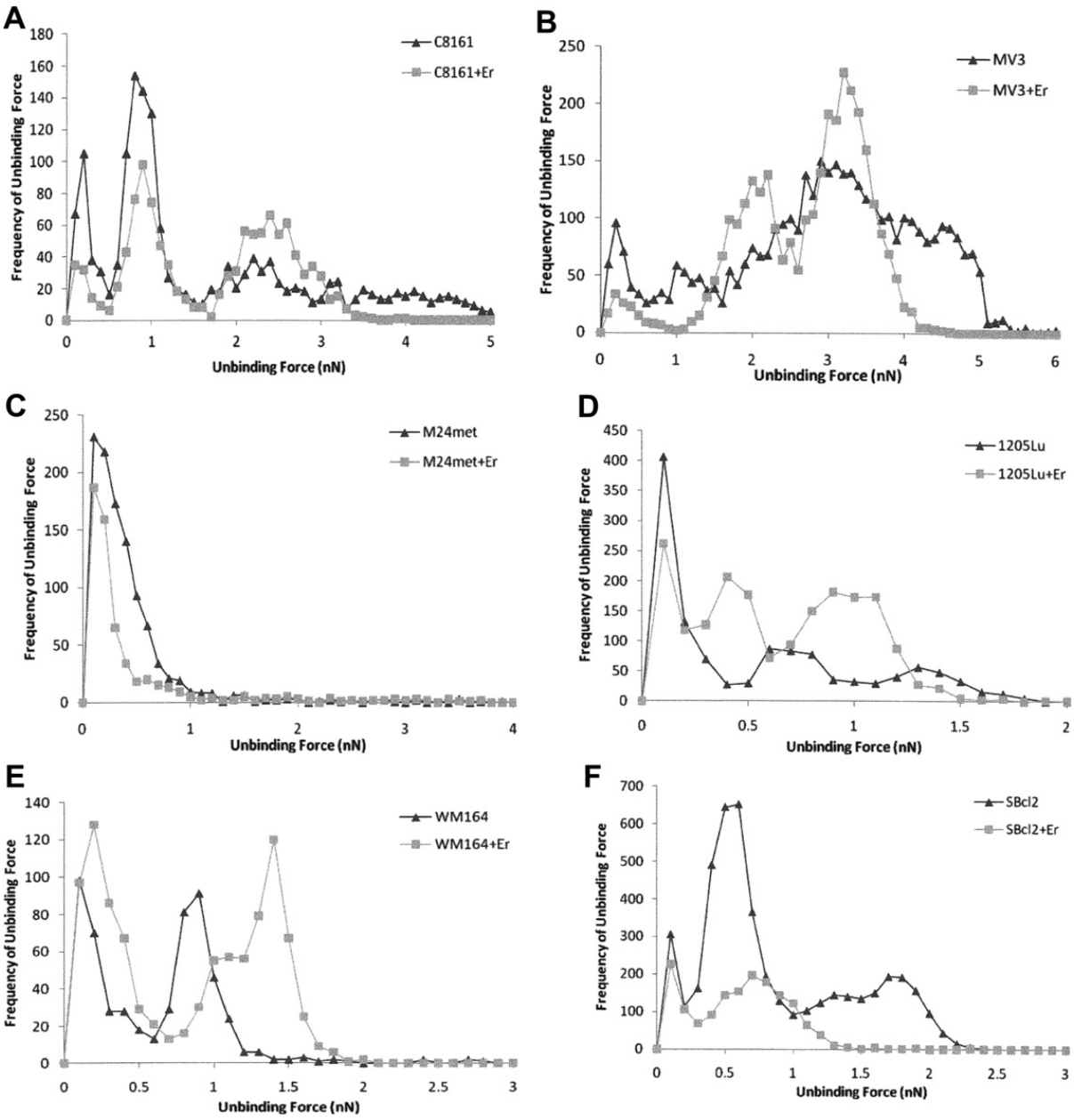

Fig. 2. Frequency of unbinding events between melanoma cells and eristostatin-functionalized AFM cantilever tips in the presence or absence of 500 nM eristostatin in at least 3 experiments; (A) C8161, (B) MV3, (C) M24met, (D) 1205Lu, (E) WM164, (F) SBcl2.

3.6. Binding of FITC-eristostatin to melanoma cells

Eristostatin binds in a dose-dependent manner to the surface of melanoma cells (Fig. 8) with only MV3 failing to show binding on its surface. However, soluble eristostatin was capable of dose-dependently inhibiting the binding of FITC-anti-$\alpha 4$ to MV3 (data not shown), indicating that eristostatin does, in fact, bind to this cell line, confirming data from Danen et al. (1998).

4. Discussion and conclusions

The uniqueness of every cancer cell line speaks to the incredible difficulty of using one treatment to affect all cancer cells. Many disintegrins such as accutin (Yeh et al., 1998), echistatin (Hallak et al., 2005; Morte et al., 2000), and contortrostatin (Markland et al., 2001; Zhou et al., 2000), have effective anti-cancer properties *in vitro* and/or *in vivo*. Often they exert their biological effect through antagonizing integrin binding, most commonly via $\alpha_v\beta_3$. This disruption can lead to inhibition of angiogenesis, induction of apoptosis, inhibition of metastasis, and tumor regression (Oliva et al., 2007). Eristostatin also has anti-cancer properties exemplified by the inhibition of lung and liver colonization, *in vivo*, of murine and human melanoma cells (Beviglia et al., 1995; Morris et al., 1995; Danen et al., 1998; McLane et al., 2003). The mechanism responsible for this effect, however, remains elusive. One aim of this study was to determine, on a binding force perspective, the characteristics of eristostatin binding on

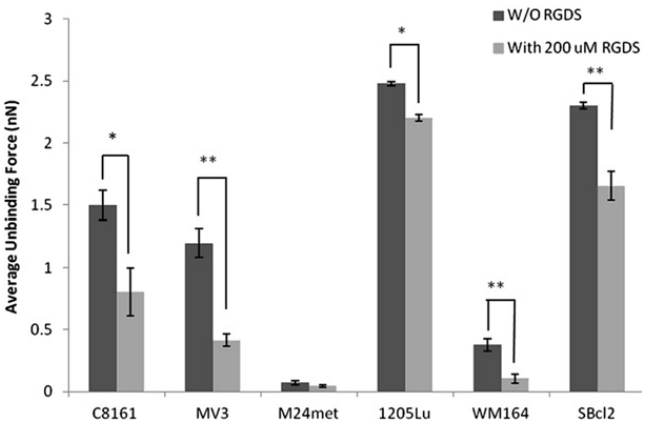

Fig. 3. Average unbinding force between melanoma cells and eristostatin on the AFM cantilever tip in the presence or absence of 200 μM synthetic RGDS peptide. Data is mean unbinding force ± SEM from at least three experiments; $^{*}p = <0.05$; $^{**}p = <0.0001$.

the melanoma surface. This study represents the first instance of testing direct disintegrin binding with the use of AFM, a powerful tool in the quantification of forces between isolated proteins and/or intact mammalian cells (Benoit and Gaub, 2002; Lehenkari and Horton, 1999; Zhang et al., 2004; Puech et al., 2006). All six human melanoma cell lines bound eristostatin to their surface (Table 1, Fig. 1). The unbinding forces observed in these experiments show an increased unbinding strength compared to those observed between the disintegrin echistatin and $\alpha_v\beta_3$ on osteoclasts (Lehenkari and Horton, 1999) or melanoma cells isolated from a vertical growth phase primary tumor, WM115, to fibronectin (Puech et al., 2006) (Table 2).

Binding of eristostatin to four of the melanoma cells' surfaces was reversible (Fig. 1); however, these results did not show complete inhibition with the addition of soluble eristostatin with any of the melanoma cells tested. In addition, 1205Lu and WM164 had no significant differences

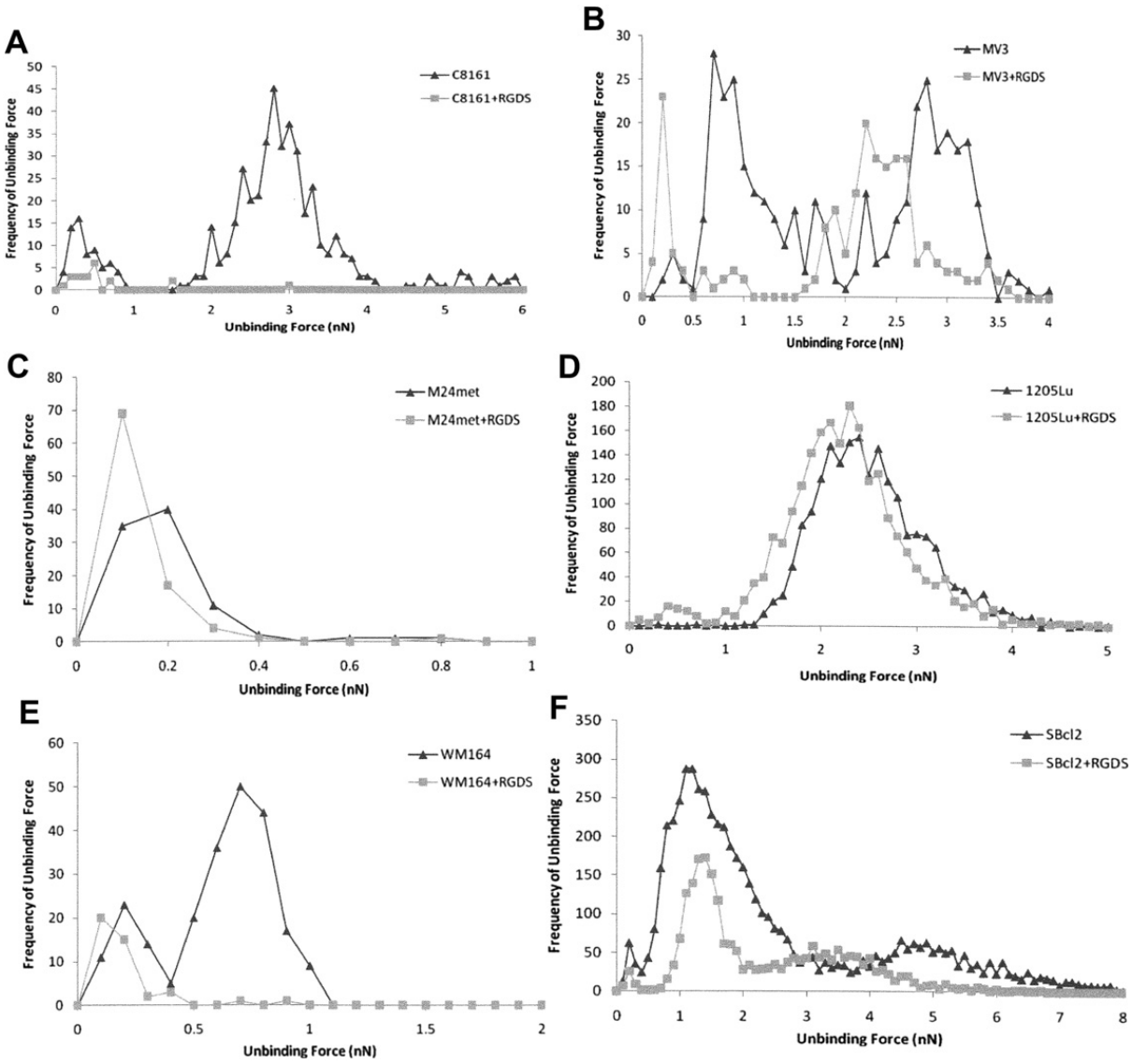

Fig. 4. Frequency of unbinding events between C8161 (A), MV3 (B), M24met (C), 1205Lu (D), WM164 (E), SBcl2 (F) and eristostatin functionalized AFM cantilever tips in the presence or absence of 200 μM RGDS peptide in at least 3 experiments.

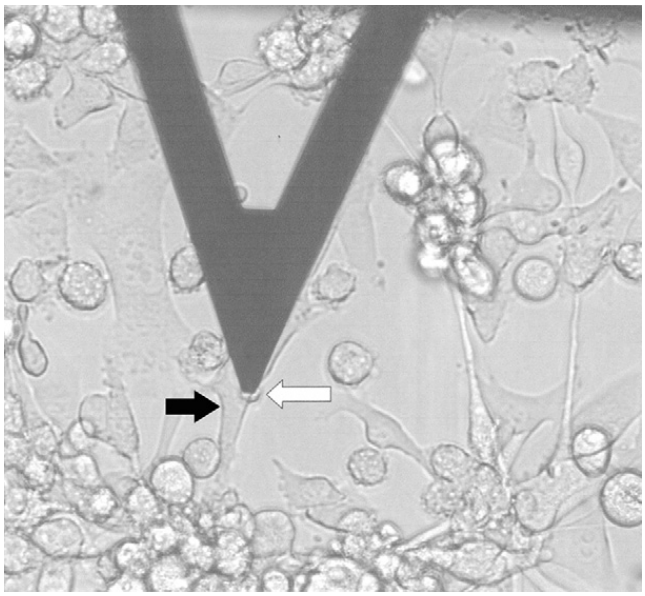

Fig. 5. Natural killer cell (white arrow) attached to tip of AFM cantilever tip engaged on WM164 human melanoma cell (black arrow) (200×).

between treatments. Both of these phenomena (partial and no inhibition) may be due to dose-dependence. Confocal data with cell lines such as 1205Lu corroborates this. Cells incubated with increasing concentrations of unlabeled eristostatin and stained with FITC-labeled eristostatin showed a reduced fluorescent signal only at the highest concentrations (1000 nM) of unlabeled eristostatin compared to controls. Therefore, higher concentrations of eristostatin may be needed in order to observe complete inhibition during AFM experiments. Interestingly, only MV3 cells did not show binding of FITC-Er to its surface by AFM, but this again may be a dose-dependence phenomenon. When Danen et al. (1998) tested FITC-Er with this cell line, the concentrations used ranged from 0 to 16,000 nM. The concentration achieved in our labeling of FITC-Er had a maximum of 93 nM, which would be insufficient to visualize binding on the MV3 cell surface, based on Danen's experiments, although it was sufficient for the other cell lines. We have, however, confirmed Er binds MV3 in a dose-dependent manner by showing a decreased surface fluorescence with labeled anti-α4 antibody with increased concentrations of unlabeled Er (data not shown).

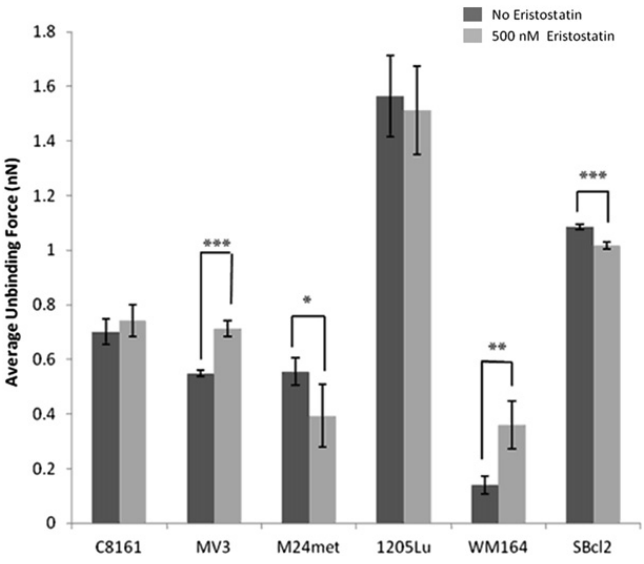

Fig. 6. Average unbinding force between melanoma cells and natural killer cells on the AFM cantilever tip. NK cell-functionalized tips were brought into contact with indicated melanoma cells incubated for 30 min in the absence (left, dark gray) or presence (right, light gray) of 500 nM eristostatin. Data is mean unbinding force ± SEM from at least three experiments; $^{*}p = <0.009$; $^{**}p = <0.0059$; $^{***}p = <0.0001$.

Histograms between eristostatin and all six melanoma cell lines revealed a common population of unbinding events in the range of 0.1–0.3 nN in both the presence and absence of eristostatin in solution. This population may be explained by intermolecular forces including electrostatic, ionic, and hydrophobic interactions present between the AFM probe and the melanoma surface (Aston and Berg, 2000; Kim et al., 2008). This intermolecular force could also be due to interactions between molecules of eristostatin which are not presented in the proper orientation or by exposed glutaraldehyde amine group ends. The method of tip functionalization which was employed in these experiments utilized glutaraldehyde as binding agent which does not bind proteins in a consistent orientation. This results in a random percentage of bound eristostatin which may not be oriented in the correct position for normal receptor interaction (Berquand and Ohler, 2010).

A second commonality which existed among most of the cell lines was the presence of a population of unbinding interactions in the 0.4–1.0 nN range. This may indicate that similar interactions are occurring between each of the melanoma cell lines comparable to measurements obtained by Puech et al. (2006) for the interaction between WM115 melanoma cells and fibronectin involving a β_1 integrin. The melanoma cell lines tested also exhibited groups of interactions at higher unbinding forces which appear to be in approximate multiples of lower forces (Fig. 2A–F). There are two ways to interpret this data. One explanation is that these data represent multiple unbinding interactions which occurred simultaneously and the summation of their unbinding strengths created an increase in affinity and thus an unbinding at higher force ranges. The AFM cantilever tip has a radius of 20 nm and eristostatin has a radius of approximately 1.1 nm (Erickson, 2009). This would allow multiple molecules of eristostatin to interact with the surface of the melanoma cell. A second explanation is that binding interactions were occurring between different receptors or surface molecules which unbind with varying force.

For this data, it cannot be determined if the observed shifts in the unbinding populations represent the same interactions at different force ranges or independent interactions; however, these most likely represent a change in the specific interactions that are occurring and not a shift in the strength of an unbinding event which has already occurred. Furthermore, it is possible that this observation may be due to the inhibition of one type of interaction by eristostatin which may then increase the prevalence or availability of a second interaction causing differences in unbinding force. We cannot at this time determine what physical changes in binding interactions result in the differences in unbinding characteristics identified in this

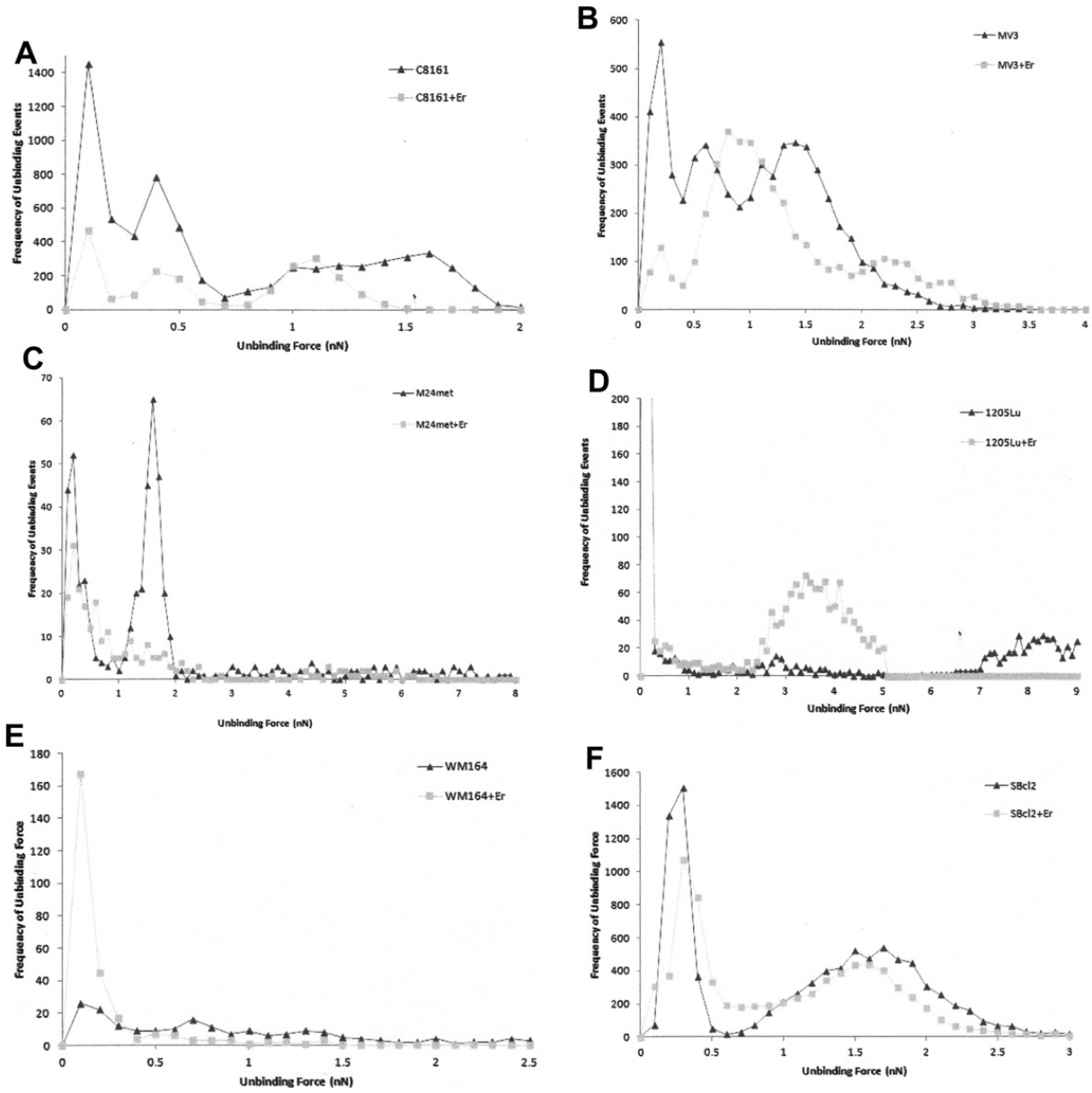

Fig. 7. Frequency of unbinding events between C8161 (A), MV3 (B), M24met (C), 1205Lu (D), WM164 (E), SBcl2 (F) and natural killer cell-functionalized AFM cantilever tips in the presence or absence of 500 nM eristostatin in at least 3 experiments.

data. It can, however, be hypothesized that the peaks at lower forces are subject to competition between soluble and tip eristostatin, whereas, unbinding populations at higher forces, which may be the result of different combinations of eristostatin–cell surface interactions, are more susceptible to conformational differences induced by soluble eristostatin. No trends or differences were observed between metastatic (C8161, MV3, M24met, and 1205Lu), vertical growth phase (WM164), and radial growth phase (SBcl2) cell lines.

AFM data using RGDS peptide as an indicator of integrin-dependence showed that only partial inhibition was reached with the addition of RGDS to the media (Figs. 3 and 4) which suggests two possible explanations. Partial inhibition could be due to concentration-dependence as mentioned previously. The second possibility is that eristostatin may not bind solely through an RGD-dependent pathway in all cell lines.

Focusing on the frequency of unbinding forces may give a better idea of the interactions that are taking place. For cell lines C8161 (Fig. 4A), MV3 (Fig. 4B), M24met (Fig. 4C), WM164 (Fig. 4E), and SBcl2 (Fig. 4F), data from RGDS blocking experiments with eristostatin-functionalized tips showed consistent populations of unbinding events similar to experiments with eristostatin on the tip in the presence of soluble eristostatin (Fig. 2). In contrast, 1205Lu (Fig. 4D) displayed different patterns of unbinding frequencies between its surface and eristostatin during experiments blocking with eristostatin versus RGDS. This may be the result of changes in integrin and cell surface receptor expression due to increased passage number which caused the cell's detachment from the plate at room temperature during later RGDS experiments. Similar morphological and physiological effects have been documented due to decreased passage number tolerance (Briske-Anderson et al., 1997). Because cells must be stationary on the

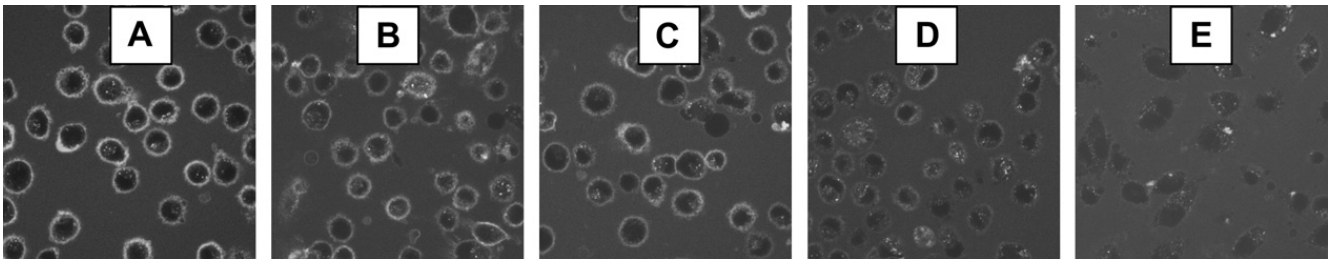

Fig. 8. Confocal images of 1205 melanoma cells (400×) stained with FITC-labeled eristostatin (A) in the presence of soluble eristostatin at 69 nM (B), 139 nM (C), 500 nM (D), and 1000 nM (E). Image backgrounds have been lightened to allow better visualization of the cell surface signals. Similar results with FITC-eristostatin were observed with C8161, WM164, M24met, SBcl2 and with FITC-anti-α4β1for MV3 (not shown).

surface to obtain accurate AFM measurements, data was only recorded from 1205Lu cells which remained attached and this may have produced bias toward one specific cell sub-population present on the plate.

C8161 (Fig. 4A) and WM164 (Fig. 4E) showed only two unbinding interactions at low and higher ranges prior to incubation with RGDS. For both cells lines the populations at the stronger forces were not observed in the presence of RGDS. This suggests that these interactions were RGD-dependent and thus most likely involved an integrin. This confirms previous data from Tian et al. (2007) in which C8161 and WM164 adhesion to an RGD matrix was disrupted by eristostatin indicating this interaction was occurring through an RGD-dependent mechanism. Comparisons between RGDS treatments among the other four cell lines indicate that this may not be the case for them. These cell lines may not be as susceptible to changes in binding interactions due to RGDS. MV3 cells (Fig. 4B) showed both decreases and increases in unbinding force frequencies at specific interaction strengths. This is consistent with data which suggests MV3 is not solely dependent on RGD binding (Tian et al., 2007). These secondary unbinding interactions may also be representative of secondary sites outside the RGD motif which may not be interrupted by a linear RGD peptide (Takagi, 2004).

Comparisons of the unbinding populations present at specific forces for each cell line show changes unique to eristostatin. In addition, alterations in interaction populations that are common for both eristostatin-blocking and RGDS-blocking experiments are present. Interaction populations at specific unbinding forces between eristostatin and the melanoma cell showed a loss or gain of a single population in the presence of both soluble eristostatin and RGDS. This provides additional evidence that these interactions are RGD-dependent and likely are due to integrin binding. In addition to this data, several populations are present in eristostatin-blocking experiments but not in RGDS-blocking experiments which may represent those interactions which are unique to eristostatin which are not dependent on the RGD motif. There were however, no major patterns between cell lines for specific populations.

Previous studies suggested that natural killer cell cytotoxicity may be responsible for the inhibitory effect that eristostatin has on melanoma cell lung colonization *in vivo*, and that eristostatin may modulate normal natural killer cell behavior (McLane et al., 2001). Here we showed that direct binding of eristostatin to the melanoma surface causes alterations in natural killer cell–melanoma cell interactions. In comparing individual interaction populations among cell lines, each cell line both lost and gained at least one unbinding population between the NK cell and the melanoma cell in the presence of soluble eristostatin with the exception of M24met which lost a population but did not gain one. It cannot yet be determined if the unbinding populations which arose in the presence of eristostatin are due to changes in surface molecule interactions (new interactions) or a result of alterations in the characteristics of interactions which had previously occurred.

These results may reflect the various changes in surface interactions between NK cells and melanoma cell due to the modulation of the presentation and density of surface molecule clustering (Mostafavi-Pour et al., 2003). The possibility also exists that eristostatin exerts a secondary effect by directly binding to natural killer cells altering the interactions between the NK cells and melanoma cells. McLane et al. (2001) determined that NK-like TALL-104

Table 1
Percentage of total contacts which showed unbinding events in the presence or absence of 500 nM eristostatin in solution with Er on the AFM tip.

Melanoma cell line	% Unbinding events	
	−Er	+Er
C8161	17.56	12.62
MV3	48.88	35.50
M24met	11.45	7.03
1205Lu	10.38	21.03
WM164	6.16	10.71
SBcl2	59.74	26.83

Table 2
Integrin surface expression repertoire on six human melanoma cell lines using flow cytometry.

Integrin subunit	Cell Line					
	C8161	MV3	M24met	1205Lu	WM164	SBcl2
α_2	+	+	nd	+	+	+
α_4	−	+	+	+	+	nd
α_{IIb}	−	−	−	−	−	−
β_1	+	+	+	+	+	+
β_3	+	−	+	+	+	−
$\alpha_v\beta_3$	+	−	+	+	+	−

+ indicates expression of integrin subunit; − indicates no expression; nd = not done.

cytotoxicity levels increased when the TALL-104 cells and melanoma cells were simultaneously treated with eristostatin in addition to the increase seen when only melanoma cells were treated. Natural killer cells can bind target cells through β_1 and β_2 integrins, including $\alpha_4\beta_1$ RGD-independent), which are selective toward multiple intercellular adhesion molecules (Genego, 2010) and are important for proper adhesion of NK cells to target cells (Chong et al., 1994; Gismondi et al., 2003; Somersalo et al., 1995). In addition to adhesion, activation of $\alpha_4\beta_1$ signaling may also cause the transcription of cytokines, such as interleukin-8, via the mitogen-activated protein kinase pathway, which plays a role in NK cytotoxicity (Mainiero et al., 1998, 2000; Chua et al., 2004). Interestingly, $\alpha_4\beta_1$ was proposed by Danen et al. (1998) as a possible target for eristostatin binding to MV3 melanoma cells. Changes in adhesion may increase interactions between NK cells and targets cells necessary for activation, and enhanced cytokine secretion would result in a rise in the immune response. These effects may be involved in eristostatin's ability to alter NK function and cytotoxicity.

One focus of this paper was determination of the RGD-dependence of the eristostatin–melanoma cell interactions. It can be questioned why specific monoclonal antibodies were not used to tease out the integrin binding specificity. There are significant limitations in the use of monoclonal antibodies in such AFM studies involving live cells, including nonspecific binding and epitope availability. Wakayama developed a method to reduce nonspecific interaction in antibody assays via AFM, but it relied on the use of detergent which would not be compatible with doing live-cell AFM testing (Wakayama et al., 2008). Studies using antibodies to examine the topology of cells have usually fixed those cells before examination (Li et al., 2012) or used cell fragments (for example, membranes as in Orsini et al., 2012). The closest to a possible experimental protocol may be attaching an antibody to the cantilever tip and exposing the tip to the surface of the melanoma or natural killer cell in the presence of unlabeled eristostatin, as modeled by Puntheeranurak et al., who probed the surface of live Chinese hamster ovary cells for antibody interactions with a sodium–glucose transporter (Puntheeranurak et al., 2006). The difference in these eristostatin experiments, however, is that the receptor (integrin or otherwise) is yet unknown and the cost for a multi-antibody screening, much less that for determining specificity, was beyond the capability of the current studies. The studies described here have shown the tantalizing complexity of cancer cell and natural killer cell interactions with a single disintegrin with known integrin selectivities, and it remains the challenge for our follow-up studies to attempt an answer to that question.

4.1. Conclusion

In order to determine the effect of eristostatin on NK cell–melanoma cell interactions, we first confirmed through AFM studies that eristostatin bound the cell surface of six melanoma cell lines. Similar interactions at 0.5–1.0 nN between all cell lines may point toward a common eristostatin binding partner, in particular a β_1-containing integrin which is part of the integrin repertoire of each melanoma cell line. Interactions with higher unbinding forces $>$0.5 nN were altered in the presence of soluble eristostatin and indicated that those populations are representative of eristostatin–melanoma surface binding. Studies using β_1 function-blocking antibodies or the utilization of siRNA to knock down the β_1 integrin subunit will be critical in determining eristostatin's binding partner.

Mean unbinding forces of eristostatin to melanoma cells also showed partial inhibition with linear RGDS peptide. C8161 and WM164 appeared to be RGD-dependent through the loss of their only major unbinding population in the presence of RGDS. The four remaining cell lines showed multiple interactions with eristostatin which were altered or remained similar with the addition of RGDS, suggesting a binding mechanism not solely dependent on the RGD motif.

Interactions between natural killer cells and melanoma cells in the presence of eristostatin showed substantial heterogeneity which affected both the frequency and force of unbinding. This result may point toward changes in surface molecule interactions (i.e. quantity and location) between NK cell and melanoma cells. In addition, the possibility of direct eristostatin–NK interactions exist which may affect natural killer cell function and cytotoxicity through downstream integrin-mediated signaling events.

Ethical statement

The work described has not been published previously (except in the form of an abstract or as part of a published lecture or academic thesis). It is not under consideration for publication elsewhere, and its publication is approved by all authors and tacitly or explicitly by the responsible authorities where the work was carried out. If accepted, it will not be published elsewhere in the same form, in English or in any other language, including electronically without the written consent of the copyright-holder.

Acknowledgments

This project was supported by grants from the National Center for Research Resources (5P20RR016472-12) and the National Institute of General Medical Sciences (8 P20 GM103446-12) from the National Institutes of Health (MAM).

Conflict of interest

There are no competing interests.

References

Aston, D.E., Berg, J.C., 2000. Long-range attraction between silanated silica materials studied by an electrolyte titration with atomic force microscopy. Colloids Surf. Physicochem. Eng. Aspect. 163, 247–263.

Benoit, M., Gaub, H.E., 2002. Measuring cell adhesion forces with the atomic force microscope at the molecular level. Cell Tissues Organs 172, 174–189.

Berquand, A., Ohler, B., 2010. Common Approaches to Tip Functionalization for AFM-base Molecular Recognition Measurements. Bruker Application Note.
Beviglia, L., Stewart, G.J., Niewiarowski, S., 1995. Effect of four disintegrins on the adhesive and metastatic properties of B16F10 melanoma cells in a murine model. Oncol. Res. 7, 7–20.
Blanchard, C.R., 1996. Atomic force microscopy. Chem. Educator 1, 1–8.
Briske-Anderson, M.J., Finley, J.W., Newman, S.M., 1997. The influence of culture time and passage number on the morphological and physiological development of Caco-2 cells. PSEBM 214, 248–257.
Cesano, A., Santoli, D., 1992. Two unique human leukemic t-cell lines endowed with a stable cytotoxic function and a different spectrum of target reactivity analysis and modulation of their lytic mechanism. In Vitro Cell. Dev. Biol. 28A, 648–656.
Chong, A.S., Boussy, I.A., Jiang, X.L., Lamas, M., Graf, L.H., 1994. CD54/ICAM-1 is a costimulator of NK cell-mediated cytotoxicity. J. Cell Immunol. 157, 92–105.
Chua, H.L., Serov, Y., Brahmi, Z., 2004. Regulation of FasL expression in natural killer cells. Hum. Immunol. 65, 317–327.
Danen, E.H.J., Marcinkiewicz, C., Cornelissen, I.M., Kraats, A.A., Pachter, J.A., Ruiter, D.J., Niewiarowski, S., Muijen, G.N.P., 1998. The disintegrin eristostatin interferes with integrin $\alpha 4\beta 1$ function and with experimental metastasis of human melanoma cells. Exp. Cell. Res., 188–196.
Dehio, M., Gomez-Duarte, O.G., Dehio, C., Meyer, T.F., 1998. Vitronectin-dependent invasion of epithelial cells by Neissera gonorrhoeae involves alpha-v integrin receptors. FEBS Lett., 84–88.
Desgrosellier, J.S., Cheresh, D.A., 2010. Integrins in cancer: biological implications and therapeutic opportunities. Natl. Rev. 10, 9–22.
Erickson, H.P., 2009. Size and shape of protein molecules at the nanometer level determined by sedimentation, gel filtration, and electron microscopy. Biol. Proced. Online 11, 32–51.
Genego, 2010. Immune Response: Role of Integrins in NK Cells Cytotoxicity [Online]. Available: http://www.genego.com/map_2228.php (01.08.11.).
Gismondi, A., Jacobelli, J., Strippoli, R., Mainiero, F., Soriani, A., Cifaldi, L., Piccoli, M., Frati, L., Santoni, A., 2003. Proline-rich tyrosine kinase 2 and Rac activation by chemokine and integrin receptors controls NK cell transendothelial migration. J. Immunol. 170, 3065–3073.
Hallak, L.K., Merchan, J.R., Storgard, C.M., Loftus, J.C., Russell, S.J., 2005. Targeted measles virus vector displaying echistatin infects endothelial cells via alpha(v)beta3 and leads to tumor regression. Cancer Res. 65, 5292–5300.
Han, W., Serry, F.M., 2008. March 25, 2008-Last Update, Force Spectroscopy with the Atomic Force Microscope [Online]. Available: http://www.afmuniversity.org/media/5989-8215EN.pdf (09.02.11.).
Howlader, N., Noone, A.M., Krapcho, M., Neyman, N., Aminou, R., Waldron, W., Altekruse, S.F., Kosary, C.L., Ruhl, J., Tatalovich, Z., Cho, H., Mariotto, A., Eisner, M.P., Lewis, D.R., Chen, H.S., Feuer, E.J., Cronin, K.A., Edwards, B.K., 2011. SEER Cancer Statistics Review, 1975-2008. National Cancer Institute, Bethesda, MD. based on November 2010 SEER data submission. Available: http://seer.cancer.gov/csr/1975_2008/.
Kim, J.S., Jung, Y.J., Park, J.W., Shaller, A.D., Wan, W., Li, A.D.Q., 2008. Mechanically stretching folded nano-Pi-stacks reveals Pico-Newton attractive forces. Adv. Mater. 20, 1–4.
Lehenkari, P.P., Horton, M.A., 1999. Single integrin molecule adhesion forces in intact cells measured by atomic force microscopy. Biochem. Biophys. Res. Commun. 259, 645–650.
Li, S., Shi, R., Wang, Q., Cai, J., Zhang, S., 2012. Nanostructure and β1-integrin distribution analysis of pig's spermatogonial stem cell by atomic force microscopy. Gene 495, 189–193.
Mainiero, F., Gismondi, A., Soriani, A., Cippitelli, M., Palmieri, G., Jacobelli, J., Piccoli, M., Frati, L., Santoni, A., 1998. Integrin-mediated ras–extracellular regulated kinase (ERK) signaling regulates interferon gamma production in human natural killer cells. J. Exp. Med. 188, 1267–1275.
Mainiero, F., Soriani, A., Strippoli, R., Jacobelli, J., Gismondi, A., Piccoli, M., Frati, L., Santoni, A., 2000. RAC1/P38 MAPK signaling pathway controls b1 integrin-induced interleukin-8 production in human natural killer cells. Immunity 12, 7–16.
Markland, F.S., Shieh, K., Zhou, Q., Golubkov, V., Sherwin, R.P., Richters, V., Sposto, R., 2001. A novel snake venom disintegrin that inhibits human ovarian cancer dissemination and angiogenesis in an orthotopic nude mouse model. Haemostasis 31, 183–191.
McCarthy, J.B., Hagen, S.T., Furcht, L.T., 1986. Human fibronectin contains distinct adhesion- and motility-promoting domains for metastatic melanoma cells. J. Cell. Biol. 102, 170–188.
McLane, M.A., Kowalska, M.A., Silver, L., Shattil, S.J., Niewiarowski, S., 1994. Interaction of disintegrins with the alpha IIb beta 3 receptor on resting and activated human platelets. Biochem. J. 301 (2), 429–436.
McLane, M.A., Kuchar, M.A., Brando, C., Santoli, D., Paquette-Straub, C.A., Miele, M.E., 2001. New insights on disintegrin-receptor interactions: eristostatin and melanoma cells. Haemostasis 31, 177–182.
McLane, M.A., Paquette-Straub, C.A., Wong, A., Srivastava, A., Miele, M.E., 2003. Effect of the disintegrin eristostatin on hematogenous metastasis in three models of human malignant melanoma. Proc. Amer. Assoc. Cancer Res., 1180.
McLane, M.A., Sanchez, E.E., Wong, A., Paquette-Straub, C., Perez, J.C., 2004. Disintegrins. Curr. Drug Targets Cardiovasc. Haematol. Disord. 4, 327–355.
Morris, V.L., Schmidt, E.E., Koop, S., MacDonald, I.C., Grattan, M., Khokha, R., McLane, M.A., Niewiarowski, S., Chambers, A.F., Groom, A.C., 1995. Effects of the disintegrin eristostatin on individual steps of hematogenous metastasis. Exp. Cell. Res. 219, 571–578.
Morte, R.D., Squillacioti, C., Garbi, C., Derkinderen, P., Belisario, M.A., Girault, J., Natale, P.D., Nitsch, L., Staiano, N., 2000. Echistatin inhibits pp125FAK autophosphorylation, paxillin phosphorylation and pp125FAK-paxillin interaction in fibronectin-adherent melanoma cells. FEBS Lett. 267, 5047–5054.
Mostafavi-Pour, Z., Askari, J.A., Parkinson, S.J., Parker, P.J., Ng, T.T.C., Humphries, M.J.1., 2003. Integrin specific signaling pathways controlling focal adhesion formation and cell migration. J. Cell. Biol. 161, 155–167.
O'Connor, R., Cesano, A., Lange, B., Fianan, J., Nowell, P.C., Clark, S.C., Raimondi, S.C., Rovera, G., Santoli, D., 1991. Growth factor requirements of childhood acute t-lymphoblastic leukemia: correlation between presence of chromosomal abnormalities and ability to grow permanently in vitro. Blood 77, 1534–1545.
Oliva, I.B., Coelho, R.M., Barcellos, G.G., Saldanha-Gama, R., Wermelinger, L.S., Marcinkiewicz, C., Benedeta Zingali, R., Barja-Fidalgo, C., 2007. Effect of RGD-disintegrins on melanoma cell growth and metastasis: involvement of the actin cytoskeleton, FAK and c-Fos. Toxicon 50, 1053–1063.
Orsini, F., Cremona, A., Arosio, P., Corsetto, P.A., Montorfano, G., Lascialfari, A., Rizzo, A.M., 2012. Atomic force microscopy imaging of lipid rafts of human breast cancer cells. Biochim. Biophys. Acta 1818, 2943–2949.
Puech, P.H., Poole, K., Knebel, D., Muller, D.J., 2006. A new technical approach to quantify cell-cell adhesion forces by AFM. Ultramicroscopy 106, 637–644.
Puntheeranurak, T., Wildling, L., Gruber, H.J., Kinne, R.K., Hinterdorfer, P., 2006. Ligands on the string: single-molecule AFM studies on the interaction of antibodies and substrates with the Na+-glucose cotransporter SGLT1 in living cells. J. Cell. Sci. 119, 2960–2967.
Rigel, S.R., Russak, J., Friedman, R., 2010. The evolution of melanoma diagnosis: 25 years beyond ABCDs. CA Cancer J. Clin. 60, 301–316.
Somersalo, K., Carpen, O., Saksela, E., Gahmberg, C.G., Nortamo, P., Timonen, T., 1995. Activation of natural killer cell migration by leukocyte integrin-binding peptide from intracellular adhesion molecule-2 (ICAM-2). J. Biol. Chem. 270, 8629–8636.
Takagi, J., 2004. Structural basis for ligand recognition by RGD (Arg-Gly-Asp)-dependent integrins. Biochem. Soc. 32, 403–406.
Tian, J., Paquette-Straub, C., Sage, E.H., Funk, S.E., Patel, V., Galileo, D., McLane, M.A., 2007. Inhibition of melanoma cell motility by the snake venom disintegrin eristostatin. Toxicon 49, 899–908.
Wakayama, J., Sekiguchi, H., Akanuma, S., Ohtani, T., Sugiyama, S., 2008. Methods for reducing nonspecific interaction in antibody-antigen assay via atomic force microscopy. Anal. Biochem. 380, 51–58.
Wierzbicka-Patynowski, I., Niewiarowski, S., Marcinkiewicz, C., Calvete, J.J., Marcinkiewicz, M.M., McLane, M.A., 1999. Structural requirements of echistatin for the recognition of alpha(v)beta(3) and alpha(5)beta(1) integrins. J. Biol. Chem. 274, 37809–37814.
Yeh, C., Peng, H., Yih, J., Huang, T., 1998. A new short chain RGD-containing disintegrin, accutin, inhibits the common pathway of human platelet aggregation. Biochim. Biophys. Acta 1425, 493–504.
Zhang, X., Chen, A., Leon, D.D., Li, H., Noiri, E., Moy, V.t., Goligorsky, M.S., 2004. Atomic force micrscopy measurment of leukocyte-endothelial interactions. Am. J. Physiol. Heart Circ. Physiol. 286, H359–H367.
Zhou, Q., Sherwin, R.P., Parrish, C., Richters, V., Groshen, S.G., Tsao-Wei, D., Markland, F.S., 2000. Contortrostatin, a dimeric disintegrin from Agkistrodon contortrix contortrix, inhibits breast cancer progression. Breast Canc. Res. Treat. 61, 249–260.
Zimmer, J. (Ed.), 2010. Natural Killer Cells: At the Forefront of Modern Immunology. Springer, Heidelberg, Germany.